ARTICLE

Bacteria activate sensory neurons that modulate pain and inflammation

Isaac M. Chiu[1], Balthasar A. Heesters[2,3], Nader Ghasemlou[1], Christian A. Von Hehn[1], Fan Zhao[4], Johnathan Tran[1], Brian Wainger[1], Amanda Strominger[1], Sriya Muralidharan[1], Alexander R. Horswill[5], Juliane Bubeck Wardenburg[6], Sun Wook Hwang[1,7], Michael C. Carroll[2] & Clifford J. Woolf[1]

Nociceptor sensory neurons are specialized to detect potentially damaging stimuli, protecting the organism by initiating the sensation of pain and eliciting defensive behaviours. Bacterial infections produce pain by unknown molecular mechanisms, although they are presumed to be secondary to immune activation. Here we demonstrate that bacteria directly activate nociceptors, and that the immune response mediated through TLR2, MyD88, T cells, B cells, and neutrophils and monocytes is not necessary for *Staphylococcus aureus*-induced pain in mice. Mechanical and thermal hyperalgesia in mice is correlated with live bacterial load rather than tissue swelling or immune activation. Bacteria induce calcium flux and action potentials in nociceptor neurons, in part via bacterial *N*-formylated peptides and the pore-forming toxin α-haemolysin, through distinct mechanisms. Specific ablation of Nav1.8-lineage neurons, which include nociceptors, abrogated pain during bacterial infection, but concurrently increased local immune infiltration and lymphadenopathy of the draining lymph node. Thus, bacterial pathogens produce pain by directly activating sensory neurons that modulate inflammation, an unsuspected role for the nervous system in host-pathogen interactions.

A dense network of low- and high-threshold sensory nerves innervate peripheral tissues including the skin, respiratory tract and gastrointestinal tract, which are often exposed to bacterial pathogens. Bacterial infection induces inflammation through immune cell recruitment[1]. Inflammatory pain during infection has been thought to be triggered by the action of immune-derived proteins (for example, cytokines and growth factors), lipids (for example, prostaglandins) and other mediators such as amines, potassium and protons on receptors expressed by nociceptors[2,3].

Staphylococcus aureus is a major cause of wound and surgical infections, leading to painful abscesses, cellulitis and necrotizing fasciitis[4,5]. *S. aureus* releases toxins including haemolysins, Panton–Valentine leukocidin and phenol soluble modulins, which have roles in bacterial dissemination and tissue damage[6–8]. We have now investigated the molecular mechanisms of pain generation during *S. aureus* infection. Unexpectedly, key immune activation pathways were not necessary for hyperalgesia during acute infection. Rather, bacteria directly activated nociceptors through *N*-formyl peptides and the pore-forming toxin α-haemolysin (αHL). Moreover, we find that nociceptors release neuropeptides that modulate innate immune activation during infection.

Pain correlates with bacterial load

To study the nature of pain caused by bacterial pathogens, we established a *S. aureus* infection model of the mouse hindpaw. Subcutaneous injection of LAC/USA300 (5×10^6 colony-forming units (c.f.u.)), a community-associated methicillin-resistant *S. aureus* strain (CA-MRSA)[8,9], resulted in mechanical, heat and cold hypersensitivity within 1 h that lasted for 48–72 h (Fig. 1a). This hyperalgesia peaked at 6 h after infection, and began to decrease at 24 h.

We quantified the kinetics of tissue swelling, immune activation and bacterial clearance. Tissue swelling did not correlate with pain, but showed an immediate peak after bacterial injection, and a second peak at 48 h after infection (Fig. 1a). Using flow cytometry, we found

increases in myeloid immune cells in infected tissues (CD11b^{+}CD45^{+}; Fig. 1b), constituted primarily of Ly6G^{+} neutrophils and Ly6C^{lo} monocytes, with fewer Ly6C^{hi} monocytes (Supplementary Fig. 1 and Fig. 1b). This influx began at 6 h, with a peak at 48 h after infection and a reduction at 72 h (Fig. 1b). Levels of CXCL1 (also called KC) and MCP-1, chemokines that mediate neutrophil/monocyte recruitment, peaked early (Supplementary Fig. 2), whereas levels of TNF-α and IL-1β, pro-inflammatory cytokines which directly sensitize nociceptors[10,11], also increased in infected tissue but did not correlate with hyperalgesia (Fig. 1c).

We next analysed live bacterial load in infected tissues. *S. aureus* recovery peaked at 6 h, and then decreased over time, similar to the time course of pain hypersensitivity (Fig. 1d). This decrease was accompanied by myeloid cell ingestion of bacteria, as detected by flow cytometry (Supplementary Fig. 1). In infected Nav1.8-Cre/TdTomato reporter mice, *S. aureus* (GFP–USA300) were often found in close proximity to dermal but not epidermal nociceptor fibres (Fig. 1e and Supplementary Fig. 3), indicating potential direct nerve–bacteria interactions. Taken together, hyperalgesia mirrors the time course of bacterial expansion and not tissue swelling or immune activation (see diagram in Supplementary Fig. 4).

Host defences not necessary for *S. aureus*-induced pain

We determined whether key immune response pathways were necessary for *S. aureus*-induced pain. Innate immune cells recognize *S. aureus*-derived cell-wall components through TLR2 (ref. 12), leading to nuclear factor-κB (NF-κB) activation through adaptor myeloid differentiation factor 88 (MyD88). TLR2 and MyD88 protect mice against *S. aureus* skin infection[4,13]. TLR3, TLR4, TLR7 and TLR9 are also functionally expressed in sensory neurons[14,15]. Thus, we analysed pain responses in $Tlr2^{-/-}$ and $Myd88^{-/-}$ mice after *S. aureus* infection. Notably, mechanical and thermal hyperalgesia were not reduced in these mice (Fig. 2a and Supplementary Fig. 5). At 72 h, $Myd88^{-/-}$

[1]Kirby Neurobiology Center, Boston Children's Hospital, and Department of Neurobiology, Harvard Medical School, Boston, Massachusetts 02115, USA. [2]Boston Children's Hospital, Program in Cellular and Molecular Medicine, and Harvard Medical School, Boston, Massachusetts 02115, USA. [3]Medical Microbiology, University Medical Center, Utrecht, Utrecht 3584 CX, The Netherlands. [4]Department of Chemistry, Quantitative Biology Program, Brandeis University, Waltham, Massachusetts 02454, USA. [5]Department of Microbiology, Roy J. and Lucille A. Carver College of Medicine, University of Iowa, Iowa City, Iowa 52242, USA. [6]Departments of Pediatrics and of Microbiology, University of Chicago, Chicago, Illinois 60637, USA. [7]Korea University Graduate School of Medicine, Seoul 136-705, South Korea.
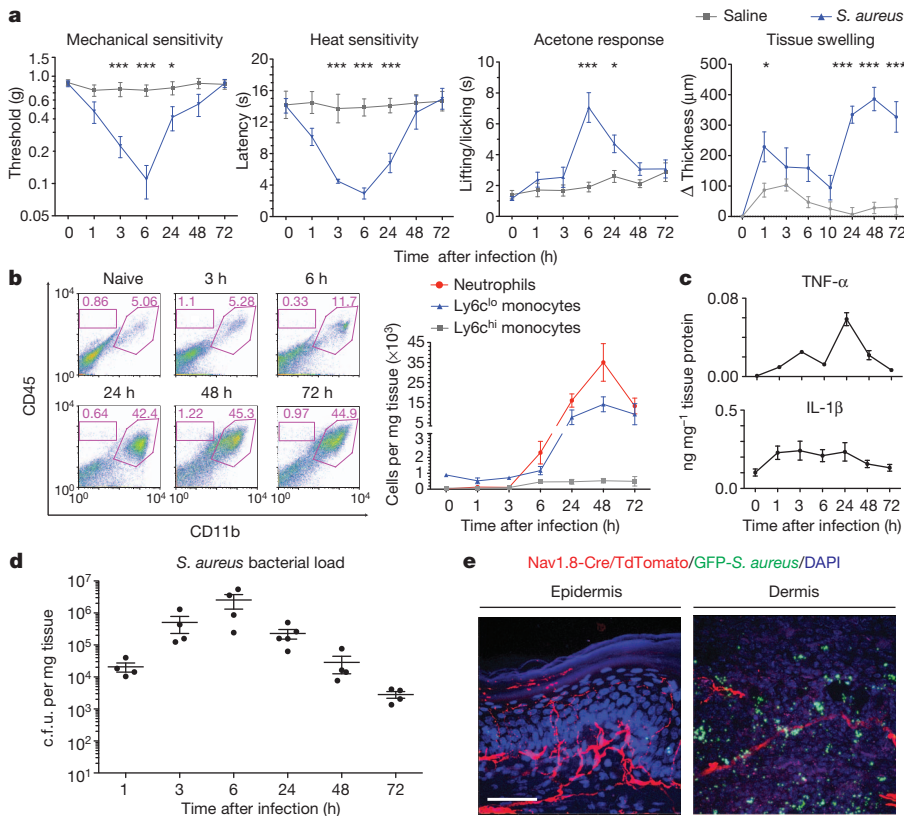
a, *S. aureus* infection induces mechanical hypersensitivity (Von Frey filaments, $P = 0.0021$, $n = 10$ per group), heat hypersensitivity (Hargreave's radiant heat test, $P < 0.0001$, $n = 10$ per group), acetone cold response (lifting/licking to acetone application, $P < 0.0001$, $n = 20$ per group) and tissue swelling ($P < 0.0001$, $n = 10$ per group). *$P < 0.05$, ***$P < 0.001$. **b**, Left: flow cytometry shows myeloid ($CD11b^+CD45^+$) but not lymphoid ($CD11b^-CD45^+$) immune expansion in infected tissues. Right: quantification of infected tissue neutrophils ($CD11b^+Ly6G^+$), $Ly6c^{hi}$ monocytes ($CD11b^+Ly6G^-Ly6C^{hi}$), and $Ly6C^{lo}$ monocytes/macrophages ($CD11b^+Ly6G^-Ly6C^{lo}$). $n = 3$ per time point. **c**, TNF-α and IL-1β levels in infected tissues. $n = 4$ per time point. **d**, Bacterial load recovery. $n = 4$ per time point. **e**, GFP–*S. aureus* are in proximity with Nav1.8-Cre/TdTomato$^+$ dermal nerve fibres, 3 h after infection. Scale bar, 100 µm. Two-way analysis of variance (ANOVA) with Bonferroni post-tests for behavioural data. Error bars indicate mean ± s.e.m.

mice showed elevated pain-like hypersensitivity, which may reflect greater bacterial load due to reduced immune activation and bacterial clearance (Fig. 2a, b).

Neutrophils and monocytes are circulating leukocytes critical for innate immunity against *S. aureus*, rapidly infiltrating sites of infection to limit pathogen survival and spread[4,16]. We treated mice with GR1 antibody before infection, which eliminated blood-borne and splenic neutrophils and monocytes (Supplementary Fig. 6). Plantar tissue-infiltrating neutrophils and monocytes during *S. aureus* infection were completely depleted by GR1 (Supplementary Fig. 7; reduction of 97% of all CD45$^+$ immune cells in infected tissues). However, instead of decreasing hyperalgesia, GR1 depletion significantly increased mechanical and heat hypersensitivity (Fig. 2c). This was accompanied by higher bacterial load, reflecting the key role of these myelomonocytic cells in combating *S. aureus* (Fig. 2d). We repeated the experiment using injection of heat-killed *S. aureus* (10^8 c.f.u.), and found that GR1 treatment decreased tissue swelling, but did not affect pain-like hypersensitivity (Supplementary Fig. 8). The increased pain during *S. aureus* infection after GR1 depletion is probably linked to uncontrolled bacterial expansion (Fig. 2d), but may also reflect neutrophil analgesic factors[17].

To analyse the contribution of the immune system to pain further, we examined *S. aureus* infection in NOD.Cg-*Prkdc^{scid} Il2rg^{tm1Wjl}*/SzJ (also called NOD scid gamma) mice, which are deficient in natural killer, T and B cells[18]. Infection-induced mechanical and heat hyperalgesia did not differ between NOD.Cg-*Prkdc^{scid} Il2rg^{tm1Wjl}*/SzJ and wild-type NOD mice (Supplementary Fig. 9). To control for strain-dependent differences, we also analysed C57BL/6 congenic *Rag1^{-/-}* mice, which are deficient in mature T and B cells[19]. Pain-like hypersensitivity did not differ after *S. aureus* infection in C57BL/6 *Rag1^{-/-}* mice compared to C57BL/6 wild-type mice (Supplementary Fig. 9). On the basis of these results, we conclude that adaptive immunity through T and B cells is not required for acute bacterial pain.

Formyl peptides and α–haemolysin activate nociceptors

The strong correlation between pain and bacterial load indicated that nociceptors directly interact with bacteria during pathogen invasion.

To test this, we applied heat-killed bacteria on dorsal root ganglia (DRG) sensory neurons. Heat-killed *S. aureus* induced a robust calcium flux response in a subset of neurons that also responded to capsaicin, which activates transient receptor potential V1 (TRPV1) (Fig. 3a). Heat-killed *S. aureus* application also induced action-potential firing in capsaicin-responsive DRG neurons (Fig. 3b). Extending these results, we found that several other strains of heat-killed bacteria caused calcium flux in DRG neurons (Fig. 3c, responsive cells: heat-killed *S. aureus* = 152 of 1,046; heat-killed *Streptococcus pneumoniae* = 82 of 968; heat-killed *Listeria monocytogenes* = 67 of 852; heat-killed *Mycoplasma fermentans* = 9 of 339; heat-killed *Helicobacter pylori* = 85 of 1,365; heat-killed *Pseudomonas aeruginosa* = 14 of 269; heat-killed *Escherichia coli* = 3 of 233). Nav1.8-Cre/TdTomato reporter mice were used to genetically mark nociceptors[20] and all bacteria-evoked neuronal responses were within the Nav1.8-Cre/TdTomato$^+$ population (Supplementary Fig. 10). Patterns of nociceptor responsiveness to particular bacteria differed, indicating strain-specific ligands acting through disparate mechanisms (Supplementary Fig. 11). Intraplantar injection of different heat-killed bacterial strains (10^8 c.f.u.) induced acute pain responses similar to the relative efficacies of nociceptor activation *in vitro* (Fig. 3d). Heat-killed *S. aureus* and heat-killed *S. pneumoniae*, which caused the most acute pain after injection, also induced mechanical and heat hyperalgesia (Supplementary Fig. 12).

We next investigated which heat-stable molecular elements within bacteria mediate nociceptor activation. Application of *S. aureus* peptidoglycans and lipoteichoic acid did not produce calcium flux in DRG neurons (Supplementary Fig. 13), and together with *in vivo* data (Fig. 2), this indicates that TLR2 ligands do not contribute significantly to *S. aureus* pain. We therefore investigated the contribution of other bacterial molecules. *N*-formylated peptides, found in bacteria and mitochondria, are recognized by G-protein-coupled formyl peptide receptors (FPRs) on leukocytes to mediate immune chemotaxis during infection[21]. Mouse vomeronasal neurons express FPRs, so may detect formyl peptides during olfaction[22,23]. We found that fMLF, an *E. coli*-derived peptide, and fMIFL, a *S. aureus*-derived peptide[24], induced calcium flux in a subset of DRG neurons that also responded
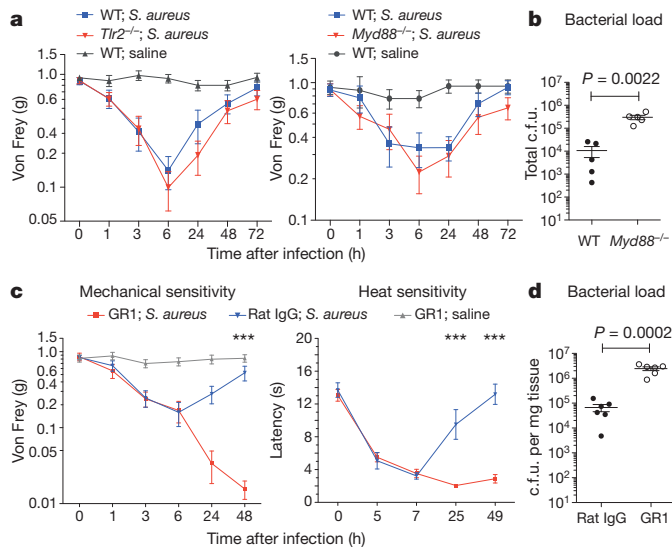
Figure 2 | Innate immunity through TLR2 and MyD88 and neutrophils and monocytes is not necessary for pain during *S. aureus* infection. a, Infection-induced mechanical hypersensitivity is similar in *Tlr2*$^{-/-}$ mice ($n = 10$ infected) compared to wild-type (WT) mice ($n = 10$ infected, $n = 10$ saline injected) ($P = 0.744$), and *Myd88*$^{-/-}$ mice ($n = 10$ infected) relative to wild-type mice ($n = 11$ infected, $n = 7$ saline injected) ($P = 0.533$). **b**, Bacterial load 3 days after infection ($n = 5$ each; P value, t-test). **c**, Infection-induced mechanical ($P < 0.0001$) and heat ($P < 0.0001$) hypersensitivity are increased in GR1-treated mice ($n = 10$ infected, $n = 10$ saline) compared to rat IgG-treated mice ($n = 10$ infected). ****P < 0.001$. **d**, Bacterial load 2 days after infection ($n = 6$ each; P value, t-test). Two-way ANOVA with Bonferroni post-tests for behavioural data. Error bars indicate mean ± s.e.m.

to capsaicin and to allyl isothiocyanate (AITC), a TRPA1 ligand (Fig. 3e and Supplementary Fig. 14). Moreover, unformylated MIFL activated fewer DRG neurons than fMIFL (Fig. 3e), similar to formyl group requirements for immune cell activation. When injected, fMLF and fMIFL induced mechanical but not heat hyperalgesia (Fig. 3f). This selective mechanical pain induction may be related to the restricted activation by formyl peptides of AITC-responsive neurons (Supplementary Fig. 14), which are mainly C-mechanosensitive fibres[25]. DRG and trigeminal ganglia express *Fpr1* and *Fpr2* (also known as *Fpr-rs2*), but not other *Fpr* genes (Supplementary Fig. 15). Microarray analysis of purified Nav1.8-Cre/TdTomato$^+$ nociceptors confirmed the specific expression of *Fpr1* but not *Fpr-rs1*, *Fpr-rs3*, *Fpr-rs4*, or *Fpr-rs7* (Supplementary Fig. 16). These data indicate that nociceptor activation may be mediated via FPR1, the receptor that recognizes fMLF and fMIFL in immune cells[24]. The FPR1 antagonist Boc-MLF reduced neuron activation by fMLF and heat-killed bacteria (Supplementary Fig. 17). *Fpr1*$^{-/-}$ mouse DRG neurons showed decreased fMIFL calcium flux, and *Fpr1*$^{-/-}$ mice showed reduced mechanical hyperalgesia after fMIFL injection relative to wild-type mice (Supplementary Fig. 17). Whereas live *S. aureus* pain peaks at 6 h, time courses may differ for heat-killed bacteria and ligands, which are influenced by ligand diffusion and clearance kinetics. Ruthenium red significantly decreased fMIFL responses in amplitude and proportion, indicating that formyl peptides may gate a downstream large-pore calcium ion channel (Supplementary Fig. 18). Heat treatment did not affect fMIFL molecular composition or the ability of fMIFL to induce hyperalgesia after injection (Supplementary Fig. 19). Notably, *Fpr1*$^{-/-}$ mice showed a reduction in mechanical but not heat hypersensitivity after injection of heat-killed *S. aureus* (Fig. 3g). Thus, formyl peptides are heat-stable elements within bacteria that contribute to the activation of mechanical hypersensitivity.

Live bacteria actively release formyl peptides[26] and secrete a host of virulence factors, including pore-forming toxins (PFTs), to facilitate tissue dissemination[6–8,27–29]. We found that *S. aureus* culture supernatant induced calcium flux in DRG neurons (Supplementary Fig. 20).
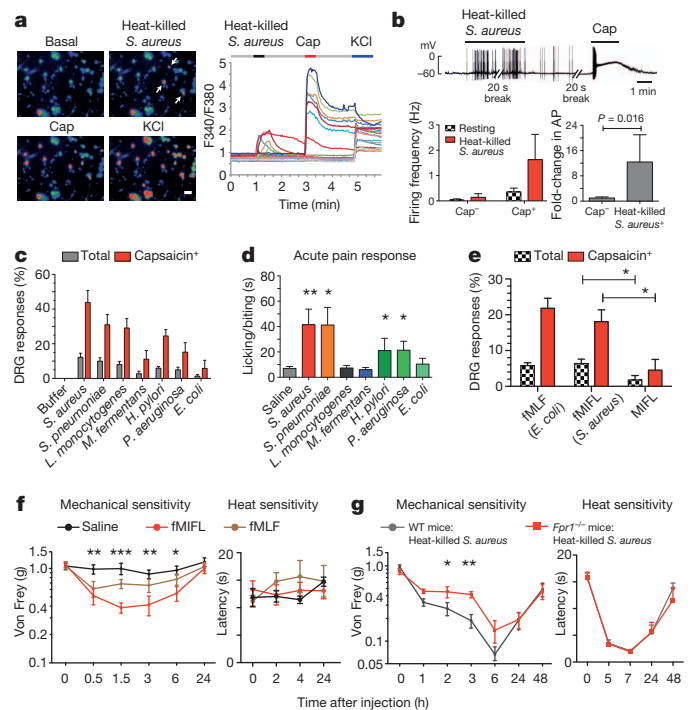
Figure 3 | Bacterial heat-stable components including *N*-formylated peptides activate nociceptors. a, Heat-killed *S. aureus* induces calcium flux in capsaicin (Cap) and KCl responsive DRG neurons (arrows, traces). **b**, Top row: representative recording; bottom row: firing frequency upon heat-killed *S. aureus* application (5 capsaicin-responsive cells, 9 unresponsive). AP, action potentials. **c**, DRG-responsive proportions to heat-killed bacteria ($n = 4–26$ fields per condition). **d**, Acute pain induction. Saline ($n = 13$), heat-killed *S. aureus* ($n = 12$), heat-killed *S. pneumoniae* ($n = 14$), heat-killed *L. monocytogenes* ($n = 5$), heat-killed *M. fermentans* ($n = 6$), heat-killed *H. pylori* ($n = 5$), heat-killed *P. aeruginosa* ($n = 8$), heat-killed *E. coli* ($n = 6$). ***P < 0.01$, *$P < 0.05$, t-test versus saline. **e**, DRG-responsive proportions to formyl peptides ($n = 3–14$ fields per condition; *$P < 0.05$, t-test). **f**, **g**, fMLF and fMIFL injection induces mechanical hypersensitivity. *Fpr1*$^{-/-}$ mice show reduced heat-killed *S. aureus* mechanical hypersensitivity ($P = 0.0089$). fMIFL versus saline and *Fpr1*$^{-/-}$ versus wild type: *$P < 0.05$; ***P < 0.01$; ****P < 0.001$. Two-way ANOVA with Bonferroni post-tests for behavioural data. Error bars indicate mean ± s.e.m.

αHL is a PFT secreted by nearly all *S. aureus* strains, and is involved in tissue damage, bacterial spread and inflammation[27–29]. When flowed onto DRG neurons, αHL induced immediate calcium flux in nociceptors, which could be washed out by buffer (Supplementary Fig. 20). αHL inserts into cell membranes and assembles into heptameric pores that allow non-selective entry of cations[29], which may be sufficient to depolarize neurons. We found that prolonged bath application of αHL on DRG neurons elicited sustained bursts of calcium flux (Fig. 4a), selectively in capsaicin-responsive neurons (Supplementary Fig. 21). αHL induced a dose-dependent calcium flux in DRG neurons (half-maximum effective concentration (EC$_{50}$) 356 nM, Fig. 4b). αHL binds to cells via A disintegrin and metalloprotease 10 (ADAM10), leading to membrane pore assembly[27,30]. ADAM10 expression was detected by PCR with reverse transcription (RT–PCR) in DRG and trigeminal ganglia (Supplementary Fig. 15). Using an antibody that recognizes the ADAM10 ectodomain, we found that a subset of Nav1.8-Cre/TdTomato$^+$ nociceptors (59.8%), but not TdTomato$^-$ cells, expressed surface ADAM10, which may contribute to selective nociceptor activation (Supplementary Fig. 22). *In vivo*, αHL injection induced significant acute pain behaviour in a dose-dependent manner (EC$_{50}$ = 6.3 pmol, Fig. 4c). Heat pre-treatment abolished the ability of αHL to induce pain (Fig. 4d), indicating that this mechanism of nociceptor activation is separate from heat-stable elements (Fig. 3). αHL also evoked action
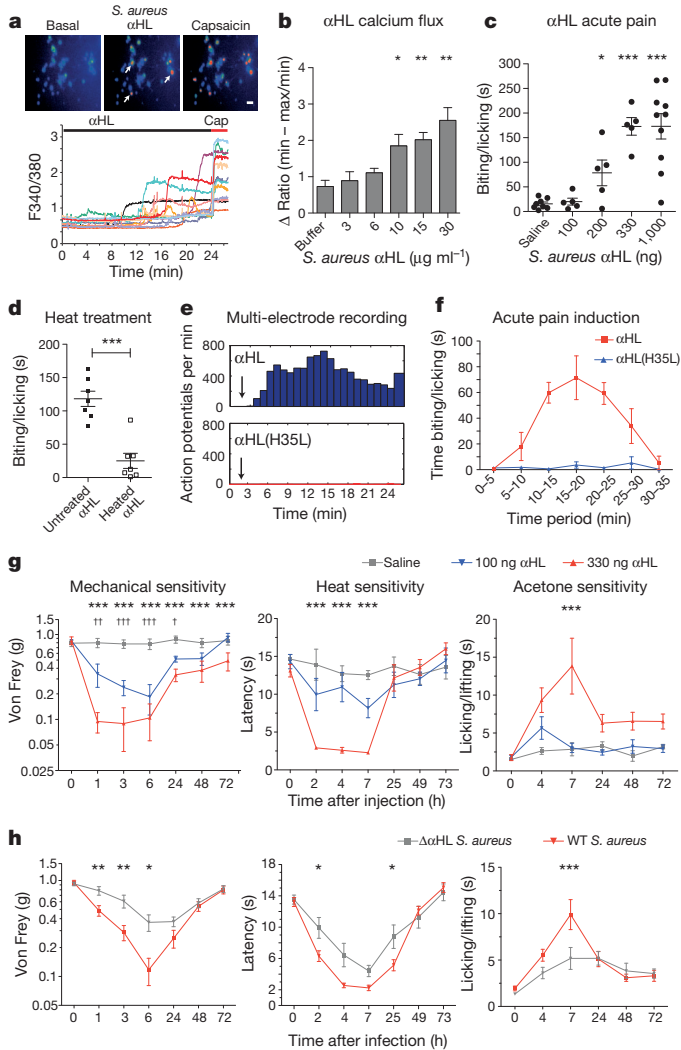
Figure 4 | Heat-sensitive *S. aureus* αHL activates nociceptors and contributes to infection-induced hyperalgesia. a–c, αHL application evoked DRG neuron calcium flux (**a**; arrows, traces), dose-dependent calcium flux (**b**; n = 3 per condition) and acute pain (**c**; n = 5–10 per group). *P < 0.05, **P < 0.01, ***P < 0.001, t-test. **d**, Heat pre-treatment abolishes αHL-induced pain (1 μg, n = 7 per group, ***P < 0.001, t-test). **e**, αHL- and αHL(H35L)-evoked DRG neuron action potentials (arrow indicates αHL application, n = 3 per condition). **f**, αHL (1 μg, n = 6) but not αHL(H35L) (1 μg, n = 5) induced acute pain. **g**, Mechanical, heat and acetone hypersensitivity induced by injection of 100 ng αHL (n = 8), 330 ng αHL (n = 8), or saline (n = 8) is shown. 100 ng αHL versus saline: ***P < 0.001; 330 ng αHL versus saline: †P < 0.05, ††P < 0.01, †††P < 0.001. **h**, *S. aureus* lacking αHL (n = 12) produced less mechanical (P = 0.0056), heat (P = 0.0193) and acetone (P = 0.0118) hypersensitivity than wild-type *S. aureus* (n = 13). *P < 0.05, **P < 0.01, ***P < 0.001. Two-way ANOVA with Bonferroni post-tests for behavioural data. Error bars indicate mean ± s.e.m.

potential firing in DRG neurons (Fig. 4e). αHL neuronal activation did not involve voltage-gated calcium channels or large-pore cation channels (not blocked by CdCl$_2$ or ruthenium red, and not absent in *Trpv1*$^{-/-}$ neurons) but did require external calcium (Supplementary Fig. 23). Therefore, αHL nociceptor activation seems to be independent of most endogenous calcium ion channels, and its ability to assemble into membrane-perforating pores may be sufficient for neuronal depolarization. H35L mutant αHL (αHL(H35L)), which cannot form a stable oligomer or pore, did not evoke action potentials (Fig. 4e) or calcium flux in DRG neurons (Supplementary Fig. 23). αHL(H35L), unlike wild-type αHL, did not produce acute pain in mice (Fig. 4f). αHL was sufficient to induce mechanical, heat and cold hypersensitivity (Fig. 4g).

Finally, we found that an isogenic *S. aureus* mutant devoid of αHL expression caused significantly less hyperalgesia than wild-type bacteria (Fig. 4h). Therefore, we conclude that αHL contributes to pain during *S. aureus* infection in a manner dependent on pore formation.

Nociceptor neuropeptides regulate inflammation

Nociceptor activation results in release of neuropeptides from peripheral terminals which can induce vasodilation and neurogenic inflammation[31]. To understand the role of nociceptors in modulating the immune response, we generated Nav1.8-Cre/diphtheria toxin A (DTA) mice to specifically ablate these cells[32]. Nav1.8-Cre/DTA DRG neurons did not show calcium flux upon stimulation with heat-killed bacteria (Fig. 5a). Mechanical and thermal hypersensitivity after *S. aureus* infection was abolished in Nav1.8-Cre/DTA mice, indicating that Nav1.8-lineage neurons are the major cell type mediating bacterial pain (Fig. 5b). Granulocytes were found 24 h after infection near Nav1.8-Cre/TdTomato$^+$ nerve fibres (Supplementary Fig. 24), and when co-cultured, DRG neurons also formed close contacts with neutrophils and macrophages (Supplementary Fig. 25), raising the question of whether nociceptors may act on immune cells. After infection, Nav1.8-Cre/DTA mice displayed significantly increased tissue swelling relative to control littermates (Fig. 5c). Bacterial load did not differ significantly between the mice (Supplementary Fig. 26). Nav1.8-Cre/DTA mice showed increased infiltration of neutrophils/monocytes at infection sites (Fig. 5d). The popliteal lymph node which drains the footpad[33] was significantly larger, by weight and cellularity, in Nav1.8-Cre/DTA mice relative to control littermates following *S. aureus* infection (Fig. 5e and Supplementary Fig. 27). There was a difference in baseline lymph node size, but the increase was substantially greater in Nav1.8-Cre/DTA than control mice after infection. Nav1.8-Cre/DTA tissues also showed increased levels of
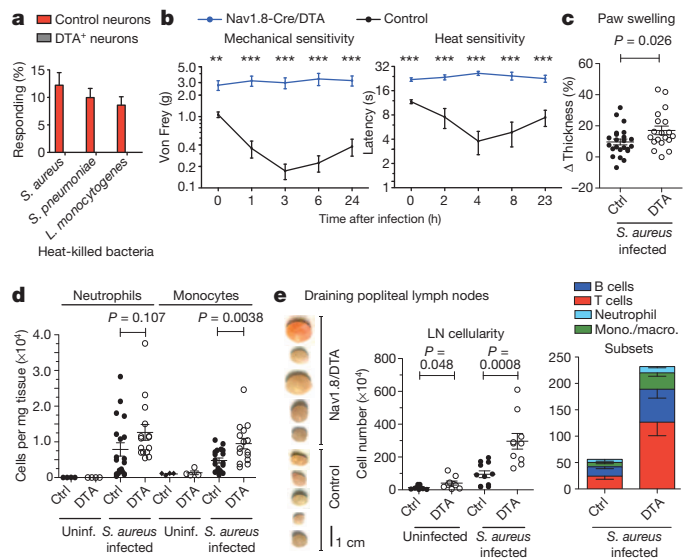
Figure 5 | Nociceptor ablation leads to increased local inflammation and lymphadenopathy after *S. aureus* infection. a, Nav1.8-Cre/DTA neurons lack heat-killed bacteria responses. **b**, Infection-induced mechanical (P = 0.0027) and heat hypersensitivity (P = 0.0003) in Nav1.8-Cre/DTA mice (n = 10 mechanical, n = 6 heat) and control littermates (n = 12 mechanical, n = 6 heat). **P < 0.01, ***P < 0.001. **c–e**, Parameters analysed 24 h after infection. **c**, Tissue swelling in Nav1.8-Cre/DTA (n = 23) and control (n = 19) mice. P value, t-test. **d**, Plantar neutrophils and monocytes: Nav1.8-Cre/DTA mice, n = 4 uninfected, n = 15 infected; control mice, n = 4 uninfected, n = 19 infected. P values, t-tests. **e**, Popliteal lymph node images (infected), lymph node cellularity (Nav1.8-Cre/DTA: n = 9 uninfected, n = 10 infected; control: n = 9 uninfected, n = 11 infected; P values, t-test) and lymph node monocyte/macrophage, neutrophil, T-cell and B-cell subsets (n = 5 each). Two-way ANOVA with Bonferroni post-tests for behavioural data. Error bars indicate mean ± s.e.m.

TNF-α (Supplementary Fig. 28), a cytokine that drives lymphadenopathy (hypertrophy) of the draining lymph node during bacterial infection[34]. This lymphadenopathy was localized, as downstream inguinal lymph nodes and spleens were not enlarged in infected Nav1.8-Cre/DTA mice (Supplementary Fig. 27). The popliteal lymphadenopathy was due to increased T cells, B cells and monocytes (Fig. 5e). Thus, nociceptor ablation led to increased local inflammation. To determine the molecular factors that mediate this immunomodulation, we performed microarray analysis of flow-cytometry-purified Nav1.8-Cre/TdTomato[+] nociceptors from dorsal root, trigeminal and nodose ganglia (Fig. 6a). Neuropeptide expression levels were ranked based on a neuropeptide database (http://www.neuropeptides.nl; Fig. 6b, full data set in Supplementary Fig. 29). Microarray data from innate immune cell subsets[35] were analysed for neuropeptide receptor levels. CGRP, galanin and somatostatin receptors showed the highest expression in neutrophils, monocytes and macrophages; these neuropeptides were also highly expressed in purified nociceptors (Fig. 6b, full data set in Supplementary Fig. 30). In vitro, we found that CGRP, galanin and somatostatin all suppressed TNF-α release from macrophages stimulated with heat-killed S. aureus or lipoteichoic acid (Fig. 6c, complete analysis in Supplementary Fig. 31). Furthermore, S. aureus supernatant and αHL induced CGRP release from DRG neurons in a dose-dependent manner (Fig. 6d). CGRP injection during S. aureus infection did not alter inflammation at the infection site, but significantly suppressed lymphadenopathy of the draining lymph nodes (Fig. 6e and Supplementary Fig. 32). Therefore, upon infection, nociceptors may release neuropeptides that directly modulate innate immune activation.

Discussion

We analysed mechanisms responsible for nociceptor activation during S. aureus infection, which commonly causes pain. We found that bacterial-derived factors directly activate nociceptors and contribute to hyperalgesia in vivo. N-formylated peptides and the PFT αHL induced direct neuronal responses through distinct mechanisms: formyl peptides through FPR1 and αHL through pore assembly leading to ionic influx (diagram, Supplementary Fig. 33).

Direct activation of nociceptors by bacteria is probably a major mechanism leading to pain, especially early in S. aureus infection during active pathogen expansion (Figs 1, 3 and 4). After immune cell infiltration, bacteria are largely eliminated, concurrent with TNF-α production, and although pain is reduced it remains (Fig. 1). Immune-mediated mechanisms may have a role during these later time points. Live infection is complex and our blockade of host defences may also enhance direct pathogen-mediated mechanisms.

Pathogen virulence and immunogenicity probably contribute to the degree of direct nociceptor activation. USA300/LAC is a highly virulent strain, expressing several PFTs in addition to αHL including β-haemolysin, γ-haemolysin, Panton–Valentine leukocidin and phenol soluble modulins[7–9]. S. aureus also possesses effective immune evasion mechanisms, including toxins that lyse immune cells, staphylococcal protein A which impairs antibody function, and complement evasion strategies[8,36]. Thus, additional elements from the bacterial proteome may exist that activate nociceptors. E. coli and other Gram-negative bacteria also induce painful infections, and lipopolysaccharides have been found to sensitize TRPV1 (ref. 15). The balance of nociceptor activation by pathogenic and immune mechanisms may differ between dissimilar pathogenic bacteria species.

Although peripheral nociceptor activation contributes to neurogenic inflammation, inducing vasodilation and capillary permeability[31], we found that ablation led to increased immune influx and lymphadenopathy, implying pain-mediated immune suppression. Our data support a role for neuropeptides in regulating innate immune activation that occurs later than the acute vascular phase of inflammation. Receptors for CGRP, galanin and somatostatin are expressed by myeloid immune subsets, and these neuropeptides have been shown to have inhibitory functions on immunity[37–39]. In particular, CGRP dampens TNF-α transcription in dendritic cells through a cAMP-dependent repressor mechanism[37,40]. CGRP downregulates cytokine levels in endotoxic shock[41], and conversely, Trpv1^{−/−} mice display increased inflammation during sepsis[42].

Potent immunomodulatory neural reflex circuits also exist that maintain immune homeostasis[43]. In Caenorhabditis elegans, a sensory neural circuit suppresses innate immunity and modulates survival during bacterial infection[44]. In mammals, vagal efferents suppress splenic macrophage activity, protecting against bacterial endotoxic shock[43,45], and activation of liver autonomic fibres modulates NK T-cell activity, leading to increased bacterial infection[34]. It has been proposed that sensory neurons initiate mammalian neural circuits[43], but a direct immunosuppressive role of nociceptive fibres, as revealed here, was not suspected. Lymph-node swelling during infection is often accompanied by pain, and nociceptor activation may limit immune influx into lymph nodes. Both nociceptive and autonomic fibres innervate lymph nodes[46]; therefore, lymph-node suppression may act through local neuropeptide release or initiation of autonomic reflex circuits. Highly pathogenic bacterial strains may have evolved the ability to exploit these neural-mediated immune regulation pathways for virulence and spread within infected tissues, by producing more nociceptor activation and greater immunosuppression.

Our data reveal an unsuspected mechanism for pain induction during bacterial infection: a direct pathogen-mediated activation of nociceptors. This neuron–pathogen interaction leads to a downregulation of the local inflammatory response. The nervous system therefore has direct sensory and modulatory roles in host–pathogen interactions during acute staphylococcal infection.
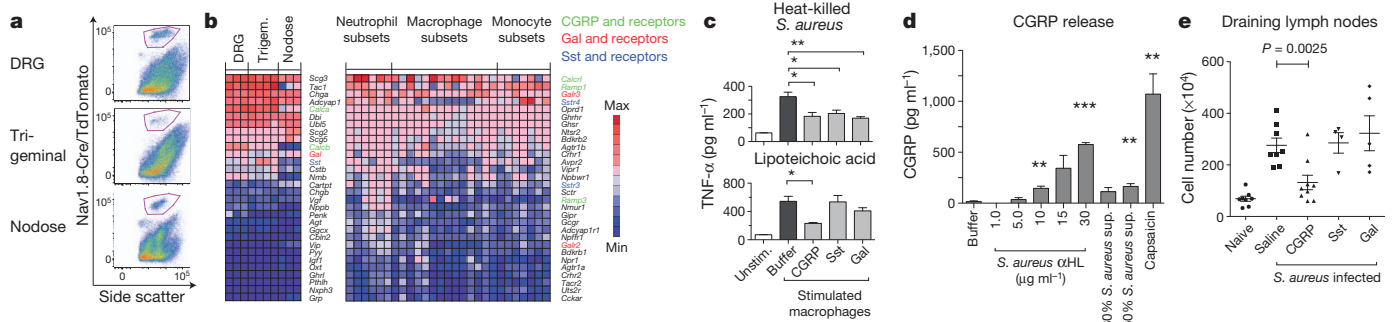
Figure 6 | Nociceptor-derived neuropeptides regulate innate immune activation. a, Nav1.8-Cre/TdTomato[+] DRG, trigeminal and nodose ganglia neurons were purified by flow cytometry (gates shown). **b**, Top 30 nociceptor-expressed neuropeptides and myeloid immune-cell-expressed neuropeptide receptors, shown from maximum to minimum. Gal, galanin; Sst, somatostatin. **c**, TNF-α production by heat-killed S. aureus or lipoteichoic-acid-stimulated macrophages was suppressed by CGRP, somatostatin and galanin (neuropeptide concentrations, 1 μM; *P < 0.05, t-test). **d**, αHL, S. aureus supernatant and capsaicin (100 nM) induce DRG neuron CGRP release. **P < 0.01, ***P < 0.001, t-test versus buffer. **e**, CGRP injection decreased lymphadenopathy 24 h after S. aureus infection. Error bars indicate mean ± s.e.m.

METHODS SUMMARY

All experiments were conducted according to institutional animal care guidelines. The following mouse strains were used: C57BL/6, C57BL/6 $Tlr2^{-/-}$, C57BL/6 $Myd88^{-/-}$, C57BL/6 $Rag1^{-/-}$, NOD wild type, NOD.Cg-$Prkdc^{scid}$ $Il2rg^{tm1Wjl}$/SzJ (Jackson Laboratories); C57BL/6 wild type, C57BL/6 $Fpr1^{-/-}$ (Taconic); Nav1.8-Cre/TdTomato, Nav1.8-Cre/DTA mice (Nav1.8-Cre (ref. 20) from R. Kuner, Heidelberg University). Bacterial strains: *S. aureus* LAC[9] and isogenic LAC deficient in αHL, described previously[6]. Recombinant αHL and αHL(H35L) are described previously[27,30]. For infection, 5×10^6 c.f.u. of *S. aureus* were injected into the plantar surface. For GFP–LAC/USA300 generation, statistical analysis, bacterial infection, formyl peptide synthesis, behaviour, microscopy, microarrays, neuronal cultures, electrophysiology, calcium imaging, flow cytometry, see Methods.

Full Methods and any associated references are available in the online version of the paper.

1. Medzhitov, R. Origin and physiological roles of inflammation. *Nature* **454**, 428–435 (2008).
2. White, R. J. Wound infection-associated pain. *J. Wound Care* **18**, 245–249 (2009).
3. Ren, K. & Dubner, R. Interactions between the immune and nervous systems in pain. *Nature Med.* **16**, 1267–1276 (2010).
4. Miller, L. S. & Cho, J. S. Immunity against *Staphylococcus aureus* cutaneous infections. *Nature Rev. Immunol.* **11**, 505–518 (2011).
5. Morgan, M. Treatment of MRSA soft tissue infections: an overview. *Injury* **42** (Suppl. 5), S11–S17 (2011).
6. Bubeck Wardenburg, J., Patel, R. J. & Schneewind, O. Surface proteins and exotoxins are required for the pathogenesis of *Staphylococcus aureus* pneumonia. *Infect. Immun.* **75**, 1040–1044 (2007).
7. Wang, R. *et al.* Identification of novel cytolytic peptides as key virulence determinants for community-associated MRSA. *Nature Med.* **13**, 1510–1514 (2007).
8. Gordon, R. J. & Lowy, F. D. Pathogenesis of methicillin-resistant *Staphylococcus aureus* infection. *Clin. Infect. Dis.* **46** (Suppl. 5), S350–S359 (2008).
9. Diep, B. A. *et al.* Complete genome sequence of USA300, an epidemic clone of community-acquired meticillin-resistant *Staphylococcus aureus*. *Lancet* **367**, 731–739 (2006).
10. Binshtok, A. M. *et al.* Nociceptors are interleukin-1β sensors. *J. Neurosci.* **28**, 14062–14073 (2008).
11. Zhang, X. C., Kainz, V., Burstein, R. & Levy, D. Tumor necrosis factor-α induces sensitization of meningeal nociceptors mediated via local COX and p38 MAP kinase actions. *Pain* **152**, 140–149 (2011).
12. Müller-Anstett, M. A. *et al.* Staphylococcal peptidoglycan co-localizes with Nod2 and TLR2 and activates innate immune response via both receptors in primary murine keratinocytes. *PLoS ONE* **5**, e13153 (2010).
13. Miller, L. S. *et al.* MyD88 mediates neutrophil recruitment initiated by IL-1R but not TLR2 activation in immunity against *Staphylococcus aureus*. *Immunity* **24**, 79–91 (2006).
14. Liu, T. *et al.* Emerging roles of toll-like receptors in the control of pain and itch. *Neurosci. Bull.* **28**, 131–144 (2012).
15. Diogenes, A. *et al.* LPS sensitizes TRPV1 via activation of TLR4 in trigeminal sensory neurons. *J. Dent. Res.* **90**, 759–764 (2011).
16. Rigby, K. M. & DeLeo, F. R. Neutrophils in innate host defense against *Staphylococcus aureus* infections. *Semin. Immunopathol.* **34**, 237–259 (2011).
17. Rittner, H. L. *et al.* Mycobacteria attenuate nociceptive responses by formyl peptide receptor triggered opioid peptide release from neutrophils. *PLoS Pathog.* **5**, e1000362 (2009).
18. Shultz, L. D. *et al.* Human lymphoid and myeloid cell development in NOD/LtSz-scid IL2Rγ null mice engrafted with mobilized human hemopoietic stem cells. *J. Immunol.* **174**, 6477–6489 (2005).
19. Mombaerts, P. *et al.* RAG-1-deficient mice have no mature B and T lymphocytes. *Cell* **68**, 869–877 (1992).
20. Agarwal, N., Offermanns, S. & Kuner, R. Conditional gene deletion in primary nociceptive neurons of trigeminal ganglia and dorsal root ganglia. *Genesis* **38**, 122–129 (2004).
21. Le, Y., Murphy, P. M. & Wang, J. M. Formyl-peptide receptors revisited. *Trends Immunol.* **23**, 541–548 (2002).
22. Liberles, S. D. *et al.* Formyl peptide receptors are candidate chemosensory receptors in the vomeronasal organ. *Proc. Natl Acad. Sci. USA* **106**, 9842–9847 (2009).
23. Rivière, S., Challet, L., Fluegge, D., Spehr, M. & Rodriguez, I. Formyl peptide receptor-like proteins are a novel family of vomeronasal chemosensors. *Nature* **459**, 574–577 (2009).
24. Southgate, E. L. *et al.* Identification of formyl peptides from Listeria monocytogenes and *Staphylococcus aureus* as potent chemoattractants for mouse neutrophils. *J. Immunol.* **181**, 1429–1437 (2008).
25. Lennertz, R. C., Kossyreva, E. A., Smith, A. K. & Stucky, C. L. TRPA1 mediates mechanical sensitization in nociceptors during inflammation. *PLoS ONE* **7**, e43597 (2012).
26. Durr, M. C. *et al.* Neutrophil chemotaxis by pathogen-associated molecular patterns–formylated peptides are crucial but not the sole neutrophil attractants produced by *Staphylococcus aureus*. *Cell. Microbiol.* **8**, 207–217 (2006).
27. Inoshima, I. *et al.* A *Staphylococcus aureus* pore-forming toxin subverts the activity of ADAM10 to cause lethal infection in mice. *Nature Med.* **17**, 1310–1314 (2012).
28. Kennedy, A. D. *et al.* Targeting of alpha-hemolysin by active or passive immunization decreases severity of USA300 skin infection in a mouse model. *J. Infect. Dis.* **202**, 1050–1058 (2010).
29. Dinges, M. M., Orwin, P. M. & Schlievert, P. M. Exotoxins of *Staphylococcus aureus*. *Clin. Microbiol. Rev.* **13**, 16–34 (2000).
30. Wilke, G. A. & Bubeck Wardenburg, J. Role of a disintegrin and metalloprotease 10 in *Staphylococcus aureus* α-hemolysin-mediated cellular injury. *Proc. Natl Acad. Sci. USA* **107**, 13473–13478 (2010).
31. Chiu, I. M., von Hehn, C. A. & Woolf, C. J. Neurogenic inflammation and the peripheral nervous system in host defense and immunopathology. *Nature Neurosci.* **15**, 1063–1067 (2012).
32. Abrahamsen, B. *et al.* The cell and molecular basis of mechanical, cold, and inflammatory pain. *Science* **321**, 702–705 (2008).
33. McLachlan, J. B. *et al.* Mast cell-derived tumor necrosis factor induces hypertrophy of draining lymph nodes during infection. *Nature Immunol.* **4**, 1199–1205 (2003).
34. Wong, C. H., Jenne, C. N., Lee, W. Y., Leger, C. & Kubes, P. Functional innervation of hepatic iNKT cells is immunosuppressive following stroke. *Science* **334**, 101–105 (2011).
35. Gautier, E. L. *et al.* Gene-expression profiles and transcriptional regulatory pathways that underlie the identity and diversity of mouse tissue macrophages. *Nature Immunol.* **13**, 1118–1128 (2012).
36. Kim, H. K., Thammavongsa, V., Schneewind, O. & Missiakas, D. Recurrent infections and immune evasion strategies of *Staphylococcus aureus*. *Curr. Opin. Microbiol.* **15**, 92–99 (2011).
37. Holzmann, B. Modulation of immune responses by the neuropeptide CGRP. *Amino Acids* **45**, 1–7 (2011).
38. Lang, R. & Kofler, B. The galanin peptide family in inflammation. *Neuropeptides* **45**, 1–8 (2010).
39. Pintér, E., Helyes, Z. & Szolcsanyi, J. Inhibitory effect of somatostatin on inflammation and nociception. *Pharmacol. Ther.* **112**, 440–456 (2006).
40. Harzenetter, M. D. *et al.* Negative regulation of TLR responses by the neuropeptide CGRP is mediated by the transcriptional repressor ICER. *J. Immunol.* **179**, 607–615 (2007).
41. Gomes, R. N. *et al.* Calcitonin gene-related peptide inhibits local acute inflammation and protects mice against lethal endotoxemia. *Shock* **24**, 590–594 (2005).
42. Fernandes, E. S. *et al.* TRPV1 deletion enhances local inflammation and accelerates the onset of systemic inflammatory response syndrome. *J. Immunol.* **188**, 5741–5751 (2012).
43. Andersson, U. & Tracey, K. J. Reflex principles of immunological homeostasis. *Annu. Rev. Immunol.* **30**, 313–335 (2012).
44. Sun, J., Singh, V., Kajino-Sakamoto, R. & Aballay, A. Neuronal GPCR controls innate immunity by regulating noncanonical unfolded protein response genes. *Science* **332**, 729–732 (2011).
45. Rosas-Ballina, M. *et al.* Acetylcholine-synthesizing T cells relay neural signals in a vagus nerve circuit. *Science* **334**, 98–101 (2011).
46. Weihe, E. *et al.* Molecular anatomy of the neuro-immune connection. *Int. J. Neurosci.* **59**, 1–23 (1991).

Supplementary Information is available in the online version of the paper.

Author Contributions I.M.C. and C.J.W. designed the study. I.M.C. and B.A.H.: infection and immune analysis; I.M.C. and N.G.: behavioural analysis; N.G. and A.S.: cytokine profiling; I.M.C. and S.M.: microscopy; I.M.C., C.A.V.H. and J.T.: neuronal culture, calcium imaging; S.W.H.: electrophysiology; F.Z.: peptide synthesis and chemistry; B.W.: multielectrode arrays. J.B.W. and A.R.H.: generation of bacterial strains; J.B.W.: recombinant αHL; J.B.W., M.C.C. and C.J.W.: supervision and expertise. I.M.C. and C.J.W. wrote the manuscript.

METHODS

Mice. C57BL/6, C57BL/6 *Tlr2*^{−/−}, C57BL/6 *Myd88*^{−/−}, C57BL/6 *Rag1*^{−/−}, C57BL/6 TdTomato reporter mice (ai14 line[47]), C57BL/6 Zsgreen mice, C57BL/6 DTA reporter mice[48], C57BL/6 *Trpv1*^{−/−} mice, NOD.Cg-*Prkdc*[scid] *Il2rg*[tm1Wjl]/SzJ and NOD wild-type mice were purchased from Jackson Laboratories; C57BL/6 *Fpr1*^{−/−}, C57BL/6 wild-type controls were purchased from Taconic Farms. Nav1.8-Cre (SNS-Cre) mice[20] were a gift from R. Kuner (University of Heidelberg). Nav1.8-Cre mice were bred with C57BL/6 TdTomato, C57BL/6 Zsgreen mice to generate Nav1.8-Cre/TdTomato and Nav1.8-Cre/Zsgreen mice. Nav1.8-Cre^{+/−} mice were bred with C57BL/6 DTA^{+/+} mice to generate nociceptor-deficient Nav1.8-Cre^{+/−}/DTA^{+/−} and control littermates (Nav1.8-Cre^{−/−}/DTA^{+/−}). For infection and behavioural experiments, adult, 7–14-week-old male mice were used, except for when age-matched, male and female Nav1.8-Cre/DTA with control littermates were used. All bacterial and animal experiments were conducted according to institutional animal care and safety guidelines and with IACUC approval at Boston Children's Hospital and Harvard Medical School.

Statistical analysis. Sample sizes for all experiments were chosen according to standard practice in the field. Bar and line graphs are plotted as mean ± standard error (s.e.m.), and in some cases, individual mice are plotted as dots. '*n*' represents the number of mice used in each group. Statistical analysis of behavioural data of mechanical, heat and cold, as well as tissue swelling time courses was conducted by two-way repeated measures ANOVA, with Bonferroni post-tests conducted for each time point tested. In these behavioural analyses, saline-injected mice or wild-type mice served as control groups for each statistical comparison.

For electrophysiology, significance was calculated using the Mann–Whitney *U*-test. Statistical comparisons of acute nocifensive behaviour (total time licking/biting in 20 min), tissue bacterial load, tissue swelling measurements, immune cell influx, neuronal responses by calcium imaging, CGRP and TNF-α levels were by unpaired, student's *t*-test. In acute pain analysis, saline-injected mice were compared to treatment groups. In CGRP and TNF analysis, buffer-treated cells were controls for comparisons. In calcium imaging, the proportion of neuronal responses from at least three fields was quantified. Data were plotted using Prism (Graphpad).

Behavioural analysis. All animals were acclimatized to the behavioural testing apparatus used on at least three habituation sessions. At least two baseline measures were obtained for each behavioural test before testing. To measure mechanical sensitivity, animals were placed on an elevated wire grid and the lateral plantar surface of the hindpaw stimulated with von Frey monofilaments (0.007–8 g). The withdrawal threshold was determined as the filament at which the animal withdrew its paw at least five in ten applications. To measure cold sensitivity, animals were placed on an elevated wire grid and a drop of acetone was applied to the plantar hindpaw by syringe. The duration of time that the animal elevated or licked the paw over a 90-s period immediately after acetone application was measured. To measure heat sensitivity, mice were plated on the glass plate of a Hargreave's apparatus set at 29 °C (IITC Life Science), and a radiant heat source applied to the plantar hindpaw. Latency to hindpaw flicking/licking was recorded (maximum of 30 s). Acute nocifensive behaviour was scored by observation of mice under a glass beaker after intraplantar injection. Time spent lifting/flinching/licking the hindpaw was recorded in 5-min intervals. Acute nocifensive behaviour was quantified as the total licking/lifting in the first 20 min after injection. In infection and compound injection experiments, observers were blinded to mouse genotype/strain. When different substances were compared within experiments, animals were randomized so similar group mean baseline thresholds were present.

Bacterial strains. *S. aureus* CA-MRSA strains LAC/USA300 and LAC/300 deficient in αHL were generated as described previously[6,27]. Strains were grown in tryptic soy broth (TSB) and tryptic soy agar (TSA) (BD Biosciences). GFP–LAC/USA300 strain AH1726 was generated by transforming GFP-expressing, chloramphenicol-resistant plasmid pCM29[49] into LAC. Plasmid DNA was electroporated into *S. aureus* as previously described[50]. The resulting strain produces GFP in a constitutive manner from the *sarA* P1 promoter, and maintained in TSB or TSA supplemented with 10 µg ml^{−1} chloramphenicol.

***S. aureus* infection model and tissue measurements.** *S. aureus* strains were grown overnight in TSB to log phase, pelleted, and re-suspended in 0.9% saline at different dilutions. OD[650] was measured to estimate bacterial density, with confirmation by TSA plating. For infection, 20 µl of bacteria (5×10^6 c.f.u.) in 0.9% saline was injected subcutaneously into the hindpaw plantar surface using a 25 µl syringe fitted with a 26-gauge needle (Hamilton Co). Mice were monitored closely after injection, and assayed for pain behaviour at different intervals. For neutrophil/monocyte depletion, mice were injected intraperitoneally (i.p.) with GR1 antibody (clone RB6-8C5, Bio-XCell) at a dose of 400 µg per 200 µl PBS, 24 h and 1 h before bacterial injections. Control rat IgG (Jackson Immunoresearch) was injected at the same dosage. For neuropeptide experiments, CGRP, galanin

and somatostatin (Tocris, doses of 1 pmol per 200 µl saline) were injected i.p. into mice at 24 h and 4 h before infection, and 4 h and 20 h after infection. As controls, saline was injected at the same time points. For tissue swelling analysis, a digital micrometer (Mitutoyo) was used to measure thickness of the plantar area before and at defined time points after infection. Thickness increase was calculated as differences from baseline measurements (or as % increase normalized to baseline). For bacterial load determination, total paw tissue from epidermis to the tendons was dissected onto ice and weighed, dissociated by dounce homogenizer (Wheaton) in 1 ml PBS, serial dilutions made, plated on TSA plates, and bacterial recovery determined by counting colonies after overnight incubation (normalized by dissected tissue weight). GFP–LAC strain was grown on TSA plates with 10 µg ml^{−1} chloramphenicol.

Neuronal cultures and calcium imaging. Dorsal root ganglia (DRG) from adult mice (7–12 weeks) were dissected into neurobasal-A medium (Life Technologies), dissociated in 1 mg ml^{−1} collagenase A plus 2.4 U ml^{−1} dispase II (enzymes, Roche Applied Sciences) in HEPES-buffered saline (Sigma) for 70 min at 37 °C. After trituration with glass Pasteur pipettes of decreasing size, DRG cells were centrifuged over a 10% BSA gradient, plated on laminin-coated cell culture dishes in B27 supplemented neurobasal-A medium plus 50 ng ml^{−1} nerve growth factor (NGF) plus penicillin/streptomycin (Life Technologies). For bacterial co-cultures, Nav1.8-Cre/TdTomato or Nav1.8-Cre/ZsGreen DRG neurons were plated in poly-lysine, laminin pre-coated, 8-well chamber slides (Lab-Tek) overnight at 37 °C. 10^6 c.f.u. GFP–*S. aureus* or CMTMR-labelled *S. pneumoniae* were added in neurobasal-A to DRG neurons for 2 h at 37 °C; co-cultures were fixed with 4% PFA and mounted in Vectashield (Vector Labs) for microscopy. DRG neurons were used for calcium imaging and electrophysiology 16–48 h after plating.

For calcium imaging, cells were loaded with 10 µM Fura-2-AM (Life Technologies) at 37 °C for 45 min in neurobasal-A medium, washed into Standard Extracellular Solution (SES, 145 mM NaCl, 5 mM KCl, 2 mM CaCl₂, 1 mM MgCl₂, 10 mM glucose, 10 mM HEPES, pH 7.5), and imaged at room temperature. Cells were illuminated by an ultraviolet light source (Xenon lamp, 75 W, Nikon), 340 nm and 380 nm excitation alternated by a LEP MAC 5000 filter wheel (Spectra services), and fluorescence emission captured by Cool SNAP ES camera (Princeton Instruments). 340/380 ratiometric images were processed, background corrected, and analysed with IPLab software (Scientific Analytics). Microsoft Excel was used for further analyses (Microsoft). Ligands were flowed directly onto neurons using perfusion barrels followed by buffer washout and further application, or applied to the culture bath at the beginning of imaging. In some experiments, 1 µM capsaicin (Tocris), 100 µM AITC (Sigma) or 40 mM KCl (Sigma) was applied after bacterial ligands.

Electrophysiology. Whole-cell transmembrane voltages of DRG neurons were recorded at room temperature (21 ± 1 °C) in the current-clamp mode using an Axopatch 200A amplifier (Molecular Devices). The internal pipette solution consisted of (in mM): 140 KCl, 5 NaCl, 2 MgCl₂, 0.5 CaCl₂, 5 EGTA, 10 HEPES, 3 Na₂ATP and 0.1 MgGTP (pH 7.4 with KOH). The extracellular solution consisted of the following: 145 NaCl, 5 KCl, 2 CaCl₂, 1 MgCl₂, 10 HEPES and 10 glucose (pH 7.4 with NaOH). Data were sampled at 5–10 kHz and analysed using pCLAMP 10.2 (Molecular Devices). Resting membrane potentials of DRG neurons were typically −60 to −65 mV and cell body diameters were 15–25 µm.

For multi-electrode arrays, DRG neurons were isolated as described, plated on MED-P515A 64-electrode probes, and recorded using a MED64 device (Alpha Med Scientific). Recombinant αHL was applied at 30 µg ml^{−1} concentration. Spikes were identified using Mobius software (Alpha Med Scientific), and histogram analysis was performed in Matlab (Mathworks).

Bacterial ligands. For heat-killed bacteria experiments, to standardize titres used for differential comparisons we used bacteria purchased from Invivogen (10^{10} c.f.u., each heat-treated for 30 min at 120 °C.): heat-killed *S. aureus*, American-type tissue culture (ATCC) strain 6539 Rosenbach; heat-killed *S. pneumoniae*, NETC7466; heat-killed *H. pylori*, ATCC strain 43504, NTCTC 11637; heat-killed *L. monocytogenes*, strain 9668P; heat-killed *M. fermentans*, ATCC strain 19989; heat-killed *P. aeruginosa*, strain ATCC strain BAA-47. For calcium imaging, bacteria were dissolved in SES at 10^7 c.f.u. ml^{−1}. We note that bacterial addition did not affect pH, which remained at pH 7.5. For injections, heat-killed bacteria strains were dissolved in 0.9% saline, 20 µl heat-killed bacteria (10^8 c.f.u. total) was injected into the hindpaw using a Hamilton syringe fitted with a 26-gauge needle.

N-formal peptides were synthesized by Foci solid-phase peptide synthesis and the peptides were formylated by 2,2,2-trifluoroethyl formate[51]. HLPC resulted in the pure compounds fMLF, fMIFL and MIFL, which were confirmed by mass spectrometry and NMR. Peptides were stored at 10 mM concentration dissolved in DMSO (Thermo Fisher) at −20 °C. For calcium imaging, fMLF, fMIFL and MIFL were dissolved in SES to 1 µM concentration. For intraplantar injections, fMLF and fMIFL were dissolved in 0.9% saline, and 1.0 µg of fMLF (2.1 nmol) or 1.3 µg of fMIFL (2.04 nmol) injected in a 20 µl volume.

For *S. aureus* supernatant collection, LAC bacteria were cultured overnight in TSB, removed by centrifugation, and resulting supernatant diluted to 5% in SES buffer for application to DRG neurons. Recombinant *S. aureus* αHL and mutant H35L (αHL(H35L)) were generated and purified as previously described[30]. Commercial αHL (Sigma) induced comparable results *in vitro* and *in vivo*. In some imaging experiments, αHL was bath applied or flowed directly onto neurons at 10 μg ml⁻¹ (Fig. 4a and Supplementary Fig. 20). For pain behavioural studies, αHL and αHL(H35L) dissolved in 0.9% saline was injected in 20 μl volume into the hindpaw at described doses. For heat inactivation, the same batch of fMIFL or recombinant αHL was split into two aliquots, one of which was treated at 100 °C for 30 min. Untreated or heat-treated substances were used for mass spectrometry and pain hypersensitivity studies.

Whole-well imaging of calcium flux. DRG neurons were seeded in B27 supplemented Neurobasal-A at 2,000 neurons per well in laminin-coated 384-well microplates (Greiner) at 37 °C for 24 h. Neurons were loaded with Fura-2 AM for 30 min at 37 °C, then washed twice with HBSS (Life Technologies). A Hamamatsu FDSS 7000EX kinetic reader was used to dispense ligands onto DRG neurons and calcium flux recorded every 1.9 s at room temperature for 30 min total. To evaluate the role of extracellular cations, cells were analysed in calcium/magnesium-free HBSS (Life Technologies). For related experiments, EDTA (5 mM) or HBSS was added to wells during recording to evaluate αHL flux.

Immune stimulation and neuroimmune co-cultures. For peritoneal macrophages, 0.5 ml Brewer's thioglycollate solution (2%) was injected i.p. into mice; 4 days later, animals were killed and peritoneal cavities flushed using 10 ml DMEM/10% fetal calf serum (FCS). Cells were plated in 96-well plates at 5,000 cells per well. For bone-marrow-derived macrophages, tibias and femurs of C57BL/6 mice were flushed using a 27 gauge needle, and bone marrow plated in 15-cm Petri dishes in DMEM/10%FCS/50 μM β-mercaptoethanol/20% L929 conditioned media for 7 days. Differentiated macrophages were dislodged from plates using non-enzymatic dissociation media in HBSS (Sigma), and plated into 96-well plates at 5,000 cells per well in DMEM/10% FCS/50 μM β-mercaptoethanol. Anti-CGRP (rat), somatostatin and galanin (Tocris) were used at different concentrations in macrophage stimulation assays. Peritoneal macrophages were stimulated with 10⁷ c.f.u. per ml heat-killed *S. aureus* (Invivogen) and bone marrow macrophages stimulated with 1 μg ml⁻¹ *S. aureus*-derived lipoteichoic acid (Invivogen) for 16 h in DMEM/10% FCS; TNF-α levels in culture supernatant were determined using an ELISA kit (Biolegend).

For neuron–macrophage co-cultures, DRG neurons were isolated and bone marrow macrophages derived as described above, re-suspended together in neurobasal-A/ 2% FCS/50 ng ml⁻¹ NGF, and co-plated at a density of 2,000 neurons + 10,000 macrophages per well into laminin/poly-D-lysine-coated 8-well chamber slides (Lab-Tek); co-cultures were fixed with 4% PFA after 20 h. For neuron–neutrophil co-cultures, DRG neurons were cultured overnight in 8-well chamber slides at 2,000 cells per well. Neutrophils were isolated as described[52,53]: briefly, bone marrow from tibias and femurs was depleted of red blood cells with ammonium-chloride-potassium buffer (0.15 M NH₄Cl, 10 mM KHCO₃, 0.1 mM EDTA), run over a discontinuous 52%, 69%, 78% percoll gradient for 30 min at 1,500*g*. The 69%/78% interface and 78% layer containing neutrophils were collected, washed, re-suspended in neurobasal medium/2% FCS/50 ng ml⁻¹ NGF and added at 10,000 cells per well to DRG neurons; co-cultures were washed and fixed with 4% PFA after 6 h. Immunostaining was performed with anti-βIII tubulin (Tuj1, 1:1,000), rat anti-CD11b (Biolegend, 1:100), followed by Alexa 568 goat anti-mouse IgG (Life Technologies, 1:500) or Alexa 488 goat anti-rat IgG (Life Technologies, 1:500), and imaged by epifluorescence microscopy.

RT–PCR and quantitative PCR. RNA was extracted from mouse bone marrow, spleen, kidneys, whole DRG, trigeminal ganglia, or DRG neurons cultured for 24 h using Qiazol reagent, followed by the RNeasy mini kit (Qiagen, MD). DNase I treatment (Qiagen) was used to remove genomic DNA, and complementary DNA reverse transcribed using Superscript III with random hexamers (Life Technologies). PCR was conducted for 32 cycles on a Mastercycler Pro thermocycler (Eppendorf), and products run on agarose gels. RT–PCR primers were synthesized by integrated DNA technologies. Primer sequences: *Adam10*, forward 5′-ATGGAG CAAACATGGCATAA-3′, reverse 5′-GCAACATCTGGGGACAAACT-3′; β-actin, forward 5′-TGTTACCAACTGGGACGACA-3′, reverse 5′-TCTCAGCTGTGG TGGTGAAG-3′; *Fpr1*, forward 5′-CAGCCTGTACTTTCGACTTCTCC-3′, reverse 5′-ATTGGTGCCTGTATCACTGGTCT-3′; *Fpr-rs1*, forward 5′-GGCAACTCT GTTGAGGAAAG-3′, reverse 5′-AATGAACTGGTTGGATTAAC-3′; *Fpr-rs2*, forward 5′-CTTTATCTGCTGGTTTCCCTTTC-3′, reverse 5′-CTGCTGCTTG AATCACTGGTTTG-3′; *Fpr-rs3*, forward 5′-TGACACCTTTAATTGCTCCT-3′, reverse 5′-GTTTCTTAATCACTCTCATTGC-3′; *Fpr-rs4*, forward 5′-CAA GAGGGGATGTGTACTGT-3′, reverse 5′-TGTTAAAGGAAGCCAAGGTA-3′; *Fpr-rs6*, forward 5′-CCCCTGAGGAGCAAGTAAAAGTAT-3′, reverse 5′-CAG GGCTGAGTCCTCCCTTA-3′; *Fpr-rs7*, forward 5′-CCTGAGGAGCAGGTAA ACATGT-3′, reverse 5′-GGGCTGAATCCTCCCTCA-3′.

For qPCR, cDNA was subjected to 2-step thermocycling using fast SYBR green master mix (Life Technologies), and data collection performed on an Applied Biosystems 7500 machine (Life Technologies). The following primers were used: *Fpr1*, forward 5′-CATTTGGTTGGTTCATGTGCAA-3′, reverse 5′-AATACAG CGGTCCAGTGCAAT-3′; *Fpr-rs2* (FPR2) was based on ref. 22, forward 5′-TGACTACTGTTAGAATTCCTG-3′, reverse 5′-GATAGCTGTGTTCAACTT TTCTTCAT-3′; *Gapdh*, forward 5′-TGGCAAAGTGGAGATTGTTGCC-3′, reverse 5′-AAGATGGTGATGGGCTTCCCG-3′. Expression levels were normalized to *Gapdh* using the ΔΔcT method.

Flow cytometry analysis of infected tissues and lymph nodes. Paw tissue was minced and digested in 1 mg ml⁻¹ collagenase A/2.4 U ml⁻¹ dispase II (Roche Applied Sciences) in HEPES buffered saline (Sigma) for 2 h at 37 °C. After digestion, cells were washed into HBSS (Life Technologies) with 0.5% bovine serum albumin (BSA, Sigma), filtered through a 70 μm mesh, re-suspended in HBSS/ 0.5% BSA, blocked with FcBlock (rat anti-CD16/CD32; 1:10 hybridoma supernatant) on ice for 5 min, and incubated with mixtures of the following antibodies: anti-CD11b-PE (Biolegend, 1:1,000), anti-CD45-PercP (Biolegend, 1:200), anti-Ly-6G-APC (Biolegend, 1:200), anti-Ly-6C-FITC (Biolegend, 1:200). Flow cytometry was conducted on a FACSCalibur machine (Bectin Dickinson) equipped with an argon and helium-neon laser.

Lymph nodes were dissected into 5 ml RPMI-1640 on ice. After dissections, RPMI-1640 was removed and replaced with 2 ml enzyme mix: RPMI-1640 containing 0.8 mg ml⁻¹ dispase + 0.2 mg ml⁻¹ collagenase P (both from Roche) plus 0.1 mg ml⁻¹ DNase I (Life Technologies). Tubes were incubated at 37 °C in a water bath and inverted at 5-min intervals to ensure well mixing. After 20 min, lymph nodes were gently aspirated and expirated using a 1-ml pipette, which disrupts the capsule to release leukocytes. The mixture was replaced in the water bath and large fragments allowed to settle for 30 s, after which the enzyme mix was removed and added to 10 ml of ice-cold FACS buffer (0.5% BSA, 2 mM EDTA, 10 mM NaN3, 15 mM HEPES in PBS, pH 7.4). 2 ml of fresh enzyme mix was added to the digestion and the process was repeated until all lymph node fragments were completely digested. Cells were filtered through 80 μm nylon mesh and counted by haemocytometer. 5×10^6 cells were incubated with 50 μl diluted antibodies (TCRβ, CD11b, Ly6C, Ly6G, CD19, antibodies from Biolegend) for 20 min at 4 °C in FACS buffer before acquisition on a FACSCalibur or FACSAria II (BD Biosciences). Neutrophils were considered CD11b⁺Ly6G⁺, monocytes CD11b⁺Ly6G⁻Ly6C⁺, B cells CD19⁺, T cells TCRβ⁺. Flow cytometry data were analysed using FlowJo software (TreeStar).

Immunostaining and microscopy. Mice were transcardially perfused with PBS followed by 4% PFA/PBS (Sigma). Plantar tissue was dissected, post-fixed for 2 h, cryoprotected in 30% sucrose/PBS, embedded, and frozen in Optimal cutting temperature compound (OCT, Electron Microscopy Sciences). Tissues were stored at −80 °C until sectioning. Cryosections were cut at 50 μm thickness onto Superfrost plus slides (Thermo Fisher). For haematoxylin and eosin, sections were dehydrated by sequential alcohol steps, mounted in Permount medium (Thermo Fisher), and imaged by light microscopy on a BZ-II analyser at ×15 magnification (Keyence). For immunostaining, sections were stained with GR1-Alexa 647 antibody (Biolegend, 1:100) for 2 h at room temperature, mounted in Vectashield with DAPI (Vector Labs) and imaged using an LSM700 laser-scanning confocal microscope (Carl Zeiss). ×10 Zeiss EC plan-NEOFLUAR dry and ×63 Zeiss plan-Apochromat oil objectives were used, with z-stacks of 40 μm total imaged at 1 μm steps; maximum projection images were exported for presentation.

For DRG, tissues were dissected, post-fixed, and embedded in OCT as described above. 14-μm cryosections were cut and stained with rabbit anti-CGRP (Millipore, PC205L, 1:500) followed by Alexa 488-anti-rabbit IgG (Life Technologies, 1:1,000) or chicken anti-neurofilament (Millipore, AB5539, 1:500), followed by Alexa 488 anti-chicken IgG (Life Technologies, 1:1,000). Sections were mounted in Vectashield with DAPI (Vector Labs), and imaged by Eclipse 50i epifluorescence microscope (Nikon).

Flow-cytometric purification of nociceptors and ADAM10 staining. DRG, trigeminal, or nodose ganglia from Nav1.8-Cre/TdTomato mice were dissected, dissociated into single cells by enzymatic digestion (1 mg ml⁻¹ collagenase A plus 2.4 U ml⁻¹ dispase II (Roche Applied Sciences) in HEPES buffered saline (Sigma)) for 60 min at 37 °C, filtered through a 70-μm filter, and stained with DAPI (Sigma, 20 ng ml⁻¹) as a dead cell stain in HBSS/0.5% BSA. Nociceptors were sorted on a FACSaria II machine (Bectin Dickinson) using a yellow–green laser to detect TdTomato fluorescence (gates, Fig. 6, Supplementary Fig. 14). To determine purity, cells were sorted into neurobasal-A and plated onto laminin-coated glass slides for microscopy. For microarrays, neurons were sorted directly into Qiazol reagent (Qiagen). For ADAM10 surface staining, Nav1.8-Cre/ TdTomato DRG were dissociated and stained with rat anti-ADAM10 ectodomain antibody (clone 139712, R&D systems; reviewed, 1DegreeBio) or with rat IgG2A isotype control (clone RTK2758, leaf purified, Biolegend) for 1 h on ice

(5 µg ml^{-1} each). After washing with HBSS, cells were incubated with Alexa 488 goat anti-rat IgG (4 µg ml^{-1}, Life technologies) for 30 min on ice. After two washes with HBSS, cells were re-suspended in HBSS/0.5% BSA and analysed on a BD FACSaria II machine. Flow cytometry data was analysed using FlowJo (Treestar).

Microarray analysis. Total RNA was extracted by sequential Qiazol extraction and purification through the RNeasy micro kit with on column genomic DNA digestion (Qiagen). RNA quality was determined by an Agilent 2100 Bioanalyzer using the RNA Pico Chip (Agilent). RNA was amplified into cDNA using the Ambion wild-type expression kit for whole transcript expression arrays, with Poly-A controls from the Affymetrix Genechip Eukaryotic Poly-A RNA control kit. The Affymetrix Genechip WT terminal labelling kit was used for fragmentation, biotin labelling. Affymetrix GeneChip Hybridization control kit and the Affymetrix GeneChip Hybridization, wash, stain kit was used to hybridize samples to Affymetrix Mouse Gene ST 1.0 GeneChips, fluidics performed on the Affymetrix Genechip Fluidics Station 450, and scanned using Affymetrix Genechip Scanner 7G (Affymetrix). Microarray work was conducted at the Boston Children's Hospital IDDRC Molecular Genetics Core, which is supported by NIH-P30-HD 18655. Affymetrix CEL files were normalized with the robust multi-array average (RMA) algorithm with quantile normalization, background correction, and median scaling. The ImmGen data set was also analysed (GEO accession number GSE15907).

Heat maps were generated using GenePattern platform (Broad institute, MIT). Nociceptor microarray data sets are deposited at the GEO database under accession number GSE46546.

47. Madisen, L. *et al.* A robust and high-throughput Cre reporting and characterization system for the whole mouse brain. *Nature Neurosci.* **13,** 133–140 (2009).
48. Voehringer, D. *et al.* Homeostasis and effector function of lymphopenia-induced ''memory-like'' T cells in constitutively T cell-depleted mice. *J. Immunol.* **180,** 4742–4753 (2008).
49. Pang, Y. Y. *et al.* agr-Dependent interactions of *Staphylococcus aureus* USA300 with human polymorphonuclear neutrophils. *J. Innate Immun.* **2,** 546–559 (2010).
50. Schenk, S. & Laddaga, R. A. Improved method for electroporation of *Staphylococcus aureus*. *FEMS Microbiol. Lett.* **94,** 133–138 (1992).
51. Hill, D. R. *et al.* 2,2,2-Trifluoroethyl fromate: a versatile and selective reagent for the formylation of alcohols, amines, and N-hydroxylamines. *Org. Lett.* **4,** 111–113 (2002).
52. Boxio, R. *et al.* Mouse bone marrow contains large numbers of functionally competent neutrophils. *J. Leukoc. Biol.* **75,** 604–611 (2004).
53. Sai, J. *et al.* Parallel phosphatidylinositol 3-kinase (PI3K)-dependent and Src-dependent pathways lead to CXCL8-mediated Rac2 activation and chemotaxis. *J. Biol. Chem.* **283,** 26538–26547 (2008).